



CHORUS

This is the accepted manuscript made available via CHORUS. The article has been published as:

Magnetotransport in metal/insulating-ferromagnet heterostructures: Spin Hall magnetoresistance or magnetic proximity effect

X. Zhou, L. Ma, Z. Shi, W. J. Fan, Jian-Guo Zheng, R. F. L. Evans, and S. M. Zhou

Phys. Rev. B **92**, 060402 — Published 4 August 2015

DOI: [10.1103/PhysRevB.92.060402](https://doi.org/10.1103/PhysRevB.92.060402)

Nature of magnetotransport in metal/insulating-ferromagnet heterostructures: Spin Hall magnetoresistance or magnetic proximity effect

X. Zhou,¹ L. Ma,¹ Z. Shi,¹ W. J. Fan,¹ Jian-Guo Zheng,² R. F. L. Evans,³ and S. M. Zhou¹

¹Shanghai Key Laboratory of Special Artificial Microstructure Materials and Technology and Pohl Institute of Solid State Physics and School of Physics Science and Engineering, Tongji University, Shanghai 200092, China

²Irvine Materials Research Institute, University of California, Irvine, CA 92697-2800, USA

³Department of Physics, University of York, York YO10 5DD, United Kingdom

(Dated: July 13, 2015)

We study the anomalous Hall-like effect (AHLE) and the effective anisotropic magnetoresistance (EAMR) in antiferromagnetic γ -IrMn₃/Y₃Fe₅O₁₂ (YIG) and Pt/YIG heterostructures. For γ -IrMn₃/YIG, the EAMR and the AHLE resistivity change sign with temperature due to the competition between the spin Hall magnetoresistance (SMR) and the magnetic proximity effect (MPE) induced by the interfacial antiferromagnetic uncompensated magnetic moment. In contrast, for Pt/YIG the AHLE resistivity changes sign with temperature whereas no sign change is observed in the EAMR. This is because the MPE and the SMR play a dominant role in the AHLE and the EAMR, respectively. As new types of galvanomagnetic property, the AHLE and the EAMR have proved vital in disentangling the MPE and the SMR in metal/insulating-ferromagnet heterostructures.

PACS numbers: 72.25.Mk, 72.25.Ba, 75.47.-m

Since the first observation of spin Hall effect (SHE) in semiconductors, it has been studied extensively because of intriguing physics and important applications in generation and detection of pure spin currents [1–4]. The SHE in heavy nonmagnetic metal (NM) strongly depends on the electronic band structure and the spin orbit coupling (SOC) [3]. The inverse spin Hall effect (ISHE) enables to electrically detect the spin current [5]. In the spin pumping technique, for example, the ISHE is employed to detect the spin current in a NM layer when the magnetization precession of a neighboring ferromagnet (FM) layer is excited [6, 7].

In their pioneering work, Nakayama *et al.* proposed spin Hall magnetoresistance (SMR) in NM/insulating-FM as a way to study the SHE in heavy NM [8]. When a charge current is applied in the NM layer, a spin current is produced along the film normal direction due to the SHE and the reflected spin current is modified by the orientation of the underlying FM magnetization with respect to the charge current. Since the reflected spin current produces an additional electric field through the ISHE, the measured resistivity of the NM layer strongly depends on the orientation of the FM magnetization [9, 10]. The longitudinal and the transverse resistivity read [8]:

$$\rho_{xx} = \rho_0 + \rho_1 m_t^2, \quad \rho_{xy} = -\rho_1 m_t m_j + \rho_2 m_n, \quad (1)$$

where m_n is the component of the magnetization unit vector along the film normal direction, and the in-plane components m_j and m_t are parallel to and perpendicular to the sensing charge current, respectively. Being negative, parameters ρ_1 and ρ_2 refer to the spin Hall induced anisotropic magnetoresistance (SH AMR) and anomalous Hall effect (SH AHE), respectively. However, Huang, Qu, Lu, and Lin *et al.* found that the magnetic proximity effect (MPE) may be involved [11–16]. For the spin polarized NM layer, the magnetoresistance (MR) effect occurs as observed in conventional

metallic FMs [17]:

$$\rho_{xx} = \rho_0 + \Delta\rho_{AMR} m_j^2, \quad \rho_{xy} = \Delta\rho_{AMR} m_t m_j + \rho_{AHE} m_n, \quad (2)$$

where ρ_{AHE} and $\Delta\rho_{AMR}$ correspond to the MPE induced anomalous Hall effect (MPE AHE) and the MPE AMR, respectively. The emerging MPE makes it complicated to clarify the mechanism of either the MR phenomena in NM/insulating-FM or the SHE in the NM layer [8–14].

With an external magnetic field H along the film normal direction, the Hall resistivity in the NM layer exhibits a similar magnetic field dependence for the AHE in bulk metallic FMs, exhibiting the anomalous Hall-like effect (AHLE). Since the MPE AHE and the SH AHE are of an *interfacial* nature, unlike the bulk feature of the conventional AHE, the AHLE is expected to bring new interesting information. For Pt/Y₃Fe₅O₁₂ (YIG) and Pd/YIG, for example, the AHLE resistivity ρ_{AHLE} changes significantly with metallic layer thickness [9, 12, 15]. Similarly, the effective AMR (EAMR) can be defined when H is rotated in the xy plane.

In this Letter, we study AHLE and EAMR in γ -IrMn₃(=IrMn)/YIG and Pt/YIG in order to separate the MPE and the SMR, where IrMn and Pt layers are antiferromagnetic and nearly ferromagnetic, respectively, exhibiting different magnetic attributes. With a strong SOC of heavy Ir atoms, a sizable SMR effect is expected in IrMn/YIG. Meanwhile, exchange bias (EB) can be established below the blocking temperature T_B by a cooling procedure under an external magnetic field parallel to the film plane and uncompensated magnetic moment may be induced [18], exhibiting an effect similar to the MPE. Accordingly, the MPE occurs at low T and disappears at high T . For Pt/YIG, however, the MPE exists at all T . The *different* T dependencies of the MPE in the two hybrid structures provide a new clue to separate the SMR and the MPE in NM/insulating-FM heterostructures.

IrMn (2.5 nm)/YIG (20 nm) and Pt (2.5 nm)/YIG (20

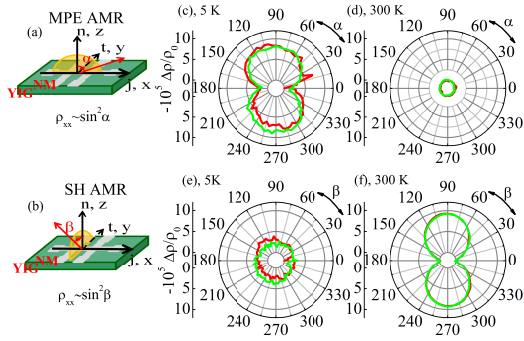


FIG. 1: Measurement geometries of the MPE AMR (a) and the SH AMR (b). In (a, b), the sensing electric current is applied along the x axis. Angular dependent $\Delta\rho/\rho_0$ in the xz (c, d) and yz (e, f) planes at 5 K (c, e) and 300 K (d, f) for IrMn/YIG. Here, the red and green lines refer to the clockwise and counter clockwise rotations of the external magnetic field $H = 10$ kOe, and $\Delta\rho = \rho_{xx} - \rho_0$.

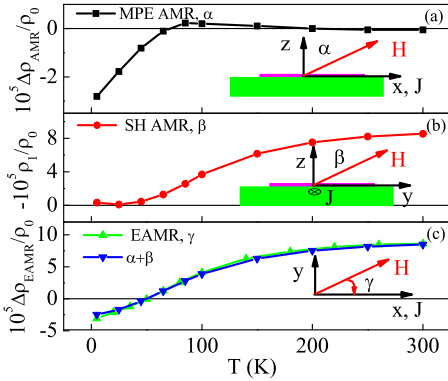


FIG. 2: For IrMn/YIG, the T dependencies of $\Delta\rho_{AMR}/\rho_0$ (a), $-\rho_1/\rho_0$ (b), and $\Delta\rho_{EAMR}/\rho_0$ (c). The data in (a, b, c) were achieved from measurements of angular dependence in xz , yz , and xy planes under $H = 10$ kOe, respectively. In (c), the sum of $-\rho_1/\rho_0$ and $\Delta\rho_{AMR}/\rho_0$ is also given.

nm) heterostructures were fabricated by pulsed laser deposition and subsequent DC magnetron sputtering on (111)-oriented, single crystalline $\text{Gd}_3\text{Ga}_5\text{O}_{12}$ substrates. Details of microstructural, magnetic, and MR measurements were described in supplementary materials [19].

When the magnetic field H is applied in the xz plane in Fig. 1(a), the longitudinal resistivity (ρ_{xx}) approximately shows the $\sin^2 \alpha$ angular dependence at low T , i.e., $\rho_{xx} \simeq \rho_0 + \Delta\rho_{AMR} \sin^2 \alpha$, but it has no variation at high T , as shown in Figs. 1(c) and 1(d). The oscillation amplitude $\Delta\rho_{AMR}$ decreases with increasing T and vanishes at high T . With $m_l \equiv 0$ in the xz plane, the SH AMR is excluded and above results arise from the MPE AMR which is in turn accompanied by EB at low T , as shown in supplementary materials [19]. Atomistic simulations[20] confirm the presence of an uncompensated magnetic moment at the IrMn/FM interface, as shown in supplementary materials [19]. Due to the structural

degradation induced by the lattice mismatch between IrMn and YIG layers, T_B of 100 K in the ultrathin IrMn layer is much lower than the Néel temperature (400-520 K) of bulk IrMn [21]. When H is rotated in the yz plane in Fig. 1(b), $m_j \equiv 0$, the MPE is excluded, and the results in Figs. 1(e) and 1(f) correspond to the SH AMR. At high T , ρ_{xx} has the $\sin^2 \beta$ angular dependence, i.e., $\rho_{xx} = \rho_0 + \rho_1 \sin^2 \beta$, whereas ρ_{xx} has no variation at low T . That is to say, the oscillatory amplitude $|\rho_1|$ increases with increasing T .

Figure 2(a) shows that the ratio $\Delta\rho_{AMR}/\rho_0$ increases from negative to positive and finally approaches zero as T changes from 5 K to 300 K. This phenomenon stems from the measurement strategy in which $\Delta\rho_{AMR}$ is obtained by the angular dependence of ρ_{xx} and contributed by three different mechanisms. Induced by the uncompensated magnetic moment, the first effect, MPE AMR, appears at low T and vanishes at $T > T_B$. The second effect is caused by the forced magnetization induced MR under high H . The uncompensated magnetic moment at finite T favors alignment under high H , leading to a negative MR. Near T_B , the second one becomes prominent and then vanishes at $T > T_B$. Caused by the ordinary MR, the third term is always positive for all T and becomes weak when the mean free path becomes short at high T . Figure 2(b) shows that the ratio $-\rho_1/\rho_0$ becomes large in magnitude at high T . Apparently, the SH AMR and the MPE AMR become strong and weak with increasing T , respectively. Interestingly, Fig. 2(c) shows that $\Delta\rho_{EAMR}/\rho_0$ measured in the xy plane in which $m_n \equiv 0$ and $m_j^2 + m_l^2 \equiv 1$, is approximately equal to the sum of $\Delta\rho_{AMR}/\rho_0$ and $-\rho_1/\rho_0$. As observed in Pd/YIG [15], one has the following equation according to Eqs. 1 and 2,

$$\Delta\rho_{EAMR} = \Delta\rho_{AMR} - \rho_1, \quad (3)$$

In particular, $\Delta\rho_{EAMR}$ also changes sign with T , indicating the competition between the MPE and the SMR.

Figure 3(a) shows that the angular dependencies of the Hall resistivity (ρ_{xy}) in the xz and yz planes are identical, in agreement with Eqs. 1 and 2. Since the ordinary Hall effect (OHE) at $H = 10$ kOe might be reasonably large, it is necessary to remove the OHE contribution from ρ_2 [10]. As shown in Fig. 3(b), for all samples the AHLE loops were measured to rigorously achieve ρ_{AHLE} . Here, $\rho_{AHLE} = (\rho_{xy+} - \rho_{xy-})/2$, where ρ_{xy+} and ρ_{xy-} are extrapolated from positive and negative saturations, respectively. As shown in supplementary materials [19], only OHE exists in single layer IrMn films. Significantly, the AHLE angle ρ_{AHLE}/ρ_0 also changes sign near $T = 100$ K, as shown in Fig. 3(c). Since ρ_2 is always negative [8], the sign change cannot be explained only in terms of the SH AHE, and the MPE AHE should also be considered according to the following equation:

$$\rho_{AHLE} = \rho_{AHE} + \rho_2. \quad (4)$$

It is revealing to analyze the physics behind the sign changes of ρ_{AHLE} and $\Delta\rho_{EAMR}$ in IrMn/YIG. The EB is

established at $T < T_B$, as shown in supplementary materials [19]. It is also evidenced by the rotational hysteresis loss between clockwise and counter clockwise curves in Figs. 1(c), 1(e), and 3(a). At low T , the AFM layer is believed to consist of rotatable and non-rotatable grains, in which AFM spins are rotated and fixed during the FM magnetization reversal process, respectively [22]. Accordingly, the MPE AHE and the MPE AMR both arise from the uncompensated magnetic moment in rotatable AFM grains at $T < T_B$ [18], and they disappear at $T > T_B$ because AFM spins in all grains are superparamagnetic, leading to vanishing uncompensated magnetic moment. This assumption was proved by atomistic calculations in supplementary materials [19]. Meanwhile, the SH AHE and the SH AMR, i.e., ρ_2 and ρ_1 , are small at low T and become large in magnitude at high T . Apparently, both ρ_{AHLE} and $\Delta\rho_{EAMR}$ are mainly contributed by the MPE at low T and the SMR at high T , respectively. Since the signs of $\Delta\rho_{AMR}$ and ρ_{AHE} are opposite to those of $-\rho_1$ and ρ_2 , the sign changes of ρ_{AHLE} and $\Delta\rho_{EAMR}$ can therefore be easily understood.

Without the data of the spin diffusion length, it is hard to separate ρ_2 and ρ_{AHE} in IrMn/YIG. At 5 K, however, $\rho_2 = 0$ is expected due to vanishing ρ_1 in Fig. 2(b), and ρ_{AHE} approximately equals the measured ρ_{AHLE} , i.e., $\rho_{AHE} \simeq \rho_{AHLE} = 2.0 \times 10^{-3} \mu\Omega\text{cm}$. The anomalous Hall conductivity (AHC) in the ultrathin IrMn layer is $\sigma_{AHC} = -0.045 \text{ S/cm}$, much smaller than the calculated results (200-400 S/cm) of bulk IrMn based on the model of non-collinear antiferromagnetism [23]. Since ρ_{AHE} at 5 K decreases sharply with the IrMn layer thickness, as shown in supplementary materials [19], the MPE AHE at low T is proved to originate from the IrMn uncompensated magnetic moment and other physical sources can be excluded. Furthermore, near $T = 300 \text{ K}$, the MPE AHE disappears and ρ_2 thus equals the measured ρ_{AHLE} , i.e., $\rho_2 \approx \rho_{AHLE} = 1.76 \times 10^{-3} \mu\Omega\text{cm}$.

Figure 4(a) shows ρ_{AHLE} and ρ_2 in Pt(2.5 nm)/YIG. Here, ρ_2 was calculated in the frame of the SMR theory [8], with the film thickness (2.5 nm) of Pt, the ratio of real and imaginary parts of the spin mixing conductance at Pt/YIG interface [10, 24], i.e., $G_i/G_r = 0.03$ and 0.06, the spin diffusion length in the inset of Fig. 4(a) [25], and the measured ρ_1 in Fig. 4(b). Since $|\rho_2| \ll |\rho_{AHLE}|$ at all T , the sign change of ρ_{AHLE} cannot be explained in terms of the SH AHE, and instead it is mainly caused by the MPE AHE according to Eq. 4. At 5 K, one has $\sigma_{AHC} = 2.0 \text{ S/cm}$. It is noted that no sign change was observed in ρ_{AHLE} for nearly-ferromagnetic-Pd/YIG [26]. The AHLE behavior in Pt/YIG is different from those of Pd/YIG [15, 26]. The T dependence of ρ_{AHLE} in NM/insulating-FM hybrid structure relies on the electronic band structures near the Fermi level [3, 27]. Shimizu *et al.*, for example, found that the T dependence of the AHLE in Pt/YIG can be tuned by the gate voltage [28]. With *ab. initio* calculation results [3, 27], the magnetic moment of Pt atoms is evaluated to be as small as $0.003 \mu_B$ with the measured $\sigma_{AHC} = 2.0 \text{ S/cm}$ at

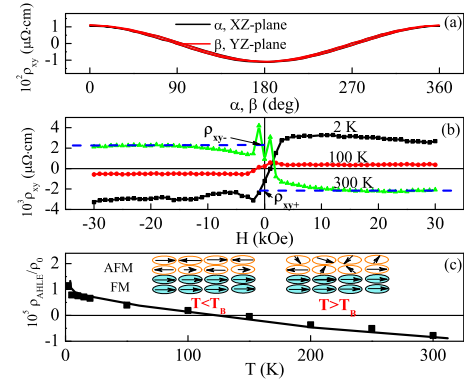


FIG. 3: For IrMn/YIG, the angular dependent ρ_{xy} in the xz (black line) and yz (red line) planes at 5 K and $H = 10 \text{ kOe}$ (a), the AHLE loops at $T = 2 \text{ K}$, 100 K, and 300 K (b), and the AHLE angle ρ_{AHLE}/ρ_0 versus T (c). The insets in (c) schematically show the IrMn spin structure below and above T_B .

5 K. Although the magnetic moment of Pt atoms depends on the chemical state on the YIG surface and the orbital hybridization of Fe and Pt atoms, it is generally smaller than the resolution ($\sim 0.01 \mu_B$) of x-ray magnetic circular dichroism and hard to be accurately detected with this technique [14, 29].

Figure 4(b) shows for Pt/YIG, $|\Delta\rho_{AMR}| \ll |\Delta\rho_{EAMR}|$ and thus $|\Delta\rho_{EAMR}| \simeq |\rho_1|$ for all T . Accordingly, Eq. 3 also holds for this system [15]. Moreover, $-\rho_1$ and $\Delta\rho_{EAMR}$, both being positive, change non-monotonically with T in Fig. 4(b), as observed in Pd/YIG and PdPt/YIG [15, 26]. This is because the SH AMR changes non-monotonically with the spin diffusion length which changes monotonically with T as shown in the inset of Fig. 4(a) [25, 30]. Consequently, $-\rho_1$ and $\Delta\rho_{EAMR}$ were also found to change non-monotonically with the Pt layer thickness [10, 12, 13]. The results in Fig. 4 unambiguously show the dominant role of the MPE (SMR) in the AHLE (EAMR) in Pt/YIG. Therefore, we have disentangled the MPE and the SMR in Pt/YIG [8–14].

It is significant to compare the SMR in IrMn/YIG and Pt/YIG. Although Pt/YIG and IrMn/YIG exhibit similar T dependent AHLE, changing sign with T , they arise from different physical mechanisms. For Pt/YIG, the sign change of the AHLE is mainly caused by the MPE AHE whereas for IrMn/YIG it is caused by the competition of the SH AHE and the MPE AHE. Moreover, the decay of the spin current in Pt and IrMn is induced by different physical mechanisms, i.e., the spin flip in Pt induced by the strong SOC and the dephasing of the spin current transverse component in IrMn [31], due to different magnetic attributes in Pt and IrMn. Therefore, the magnitude of the spin diffusion length and its T dependence may be different in IrMn and Pt. It is shorter than 1.0 nm for IrMn and 0.5-3.4 nm for Pt at 300 K [32, 33]. Accordingly, ρ_1 in IrMn/YIG and Pt/YIG exhibits different variation trends with T , as shown in Fig. 2(b) and Fig. 4(b). With measured ρ_1 and ρ_2 at 300 K for

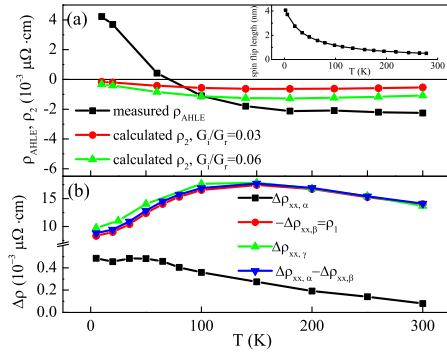


FIG. 4: For Pt/YIG, the T dependencies of measured ρ_{AHLE} and calculated ρ_2 (a), and of $\Delta\rho_{AMR}$ (MPE AMR), $-\rho_1$ (SH AMR), and $\Delta\rho_{EAMR}$ (EAMR) measured by the angular dependence of ρ_{xx} in the xz , yz , and xy planes under $H = 10$ kOe (b). In the inset of (a), the spin flip length of Pt is taken from Ref. 25. For comparison, the sum of $\Delta\rho_{AMR}$ and $-\rho_1$ is also given in (b).

IrMn/YIG in Figs. 2(b) and 3(c), the ratio G_i/G_r is evaluated to be 0.12, larger than that (0.03 and 0.06) of Pt/YIG [10, 24]. With $G_r(\text{IrMn/YIG})/G_r(\text{Pt/YIG}) = 0.43$ [34], one can see that $G_i(\text{IrMn/YIG})$ is larger than that of $G_i(\text{Pt/YIG})$ by a factor of 1.7. Since the G_i reflects the phase shift of the reflection coefficients between spin-up and spin-down at the interface, the larger G_i in IrMn/YIG may come from the tuning of AFM spin structure by the neighboring FM spins through the interfacial exchange coupling [31]. Moreover, the smaller $G_r(\text{IrMn/YIG})$ might be caused by the less channels in IrMn, compared with Pt [35, 36]. Finally, the spin Hall angle at 300 K is reported to be about 0.028 for IrMn, smaller than that of 0.056 for Pt [32, 34].

In summary, the SMR and the MPE are both experimentally proved to be important in the mixed MR behavior. For IrMn/YIG, both ρ_{AHLE} and $\Delta\rho_{EAMR}$ change sign with T due to the competition between the SMR and the MPE. For Pt/YIG, the sign change is observed only in ρ_{AHLE} because the SH AHE/SH AMR is much weaker/stronger than the MPE AHE/MPE AMR. Moreover, the galvanomagnetic properties in NM/insulating-FM strongly depend on the magnetic attribute of metallic layers. The MPE in IrMn can be switched on/off by tuning the temperature, which is helpful for design and fabrication of state-of-the-art antiferromagnetic spintronic devices. Quite notably, the AHLE and the EAMR will facilitate both full understanding of the intricate MR in NM/insulating-FM and better characterization of functionality and performance in spin current devices.

This work was supported by the State Key Project of Fundamental Research Grant No. 2015CB921501, the National Science Foundation of China Grant Nos. 11374227, 51331004, 51171129, and 51201114, Shanghai Science and Technology Committee Nos. 0252nm004, 13XD1403700, and 13520722700. TEM specimen preparation and observation was performed at the Irvine Materials Research Institute

at UC Irvine, using instrumentation funded in part by the National Science Foundation Center for Chemistry at the Space-Time Limit under grant no. CHE-0802913

- [1] Y. K. Kato, R. C. Myers, A. C. Gossard, and D. D. Awschalom, *Science* **306**, 1910(2004)
- [2] J. Wunderlich, B. Kaestner, J. Sinova, and T. Jungwirth, *Phys. Rev. Lett.* **94**, 047204(2005)
- [3] G. Y. Guo, S. Murakami, T. W. Chen, and N. Nagaosa, *Phys. Rev. Lett.* **100**, 096401(2008)
- [4] W. Zhang, M. B. Jungfleisch, W. J. Jiang, J. E. Pearson, A. Hoffmann, F. Freimuth, and Y. Mokrousov, *Phys. Rev. Lett.* **113**, 196602(2014)
- [5] S. O. Valenzuela and M. Tinkham, *Nature (London)* **442**, 176 (2006)
- [6] K. Ando, S. Takahashi, J. Ieda, H. Kurebayashi, T. Trypiniotis, C. H. W. Barnes, S. Maekawa, and E. Saitoh, *Nat. Mater.* **10**, 655 (2011)
- [7] F. D. Czeschka, L. Dreher, M. S. Brandt, M. Weiler, M. Althammer, I. M. Imort, G. Reiss, A. Thomas, W. Schoch, W. Limmer, H. Huebl, R. Gross, and S. T. B. Goennenwein, *Phys. Rev. Lett.* **107**, 046601(2011)
- [8] H. Nakayama, M. Althammer, Y. T. Chen, K. Uchida, Y. Kajiwara, D. Kikuchi, T. Ohtani, S. Geprags, M. Opel, S. Takahashi, R. Gross, G. E. W. Bauer, S. T. B. Goennenwein, and E. Saitoh, *Phys. Rev. Lett.* **110**, 206601(2013)
- [9] N. Vlietstra, J. Shan, V. Castel, B. J. van Wees, and J. Ben Youssef, *Phys. Rev. B* **87**, 184421 (2013)
- [10] M. Althammer, S. Meyer, H. Nakayama, M. Schreier, S. Altmannshofer, M. Weiler, H. Huebl, S. Geprags, M. Opel, R. Gross, D. Meier, C. Klewe, T. Kuschel, J. M. Schmalhorst, G. Reiss, L. M. Shen, A. Gupta, Y. T. Chen, G. E. W. Bauer, E. Saitoh, and S. T. B. Goennenwein, *Phys. Rev. B* **87**, 224401(2013)
- [11] S. Y. Huang, W. G. Wang, S. F. Lee, J. Kwo, and C. L. Chien, *Phys. Rev. Lett.* **107**, 216604(2011)
- [12] S. Y. Huang, X. Fan, D. Qu, Y. P. Chen, W. G. Wang, J. Wu, T. Y. Chen, J. Q. Xiao, and C. L. Chien, *Phys. Rev. Lett.* **109**, 107204(2012)
- [13] D. Qu, S. Y. Huang, J. Hu, R. Q. Wu, and C. L. Chien, *Phys. Rev. Lett.* **110**, 067206(2013)
- [14] Y. M. Lu, Y. Choi, C. M. Ortega, X. M. Cheng, J. W. Cai, S. Y. Huang, L. Sun, and C. L. Chien, *Phys. Rev. Lett.* **110**, 147207(2013)
- [15] T. Lin, C. Tang, H. M. Alyahayaei, and J. Shi, *Phys. Rev. Lett.* **113**, 037203 (2014)
- [16] B. F. Miao, S. Y. Huang, D. Qu, and C. L. Chien, *Phys. Rev. Lett.* **112**, 236601(2014)
- [17] T. R. Mcguire and R. I. Potter, *IEEE Trans. Magn.* **11**, 1018(1975)
- [18] X. Zhang and L. K. Zou, *Appl. Phys. Lett.* **105**, 262401(2014)
- [19] See supplemental materials for fabrication, microstructural characterization, exchange bias, atomistic simulations of the interfacial moment IrMn/YIG bilayer, AHC of IrMn/YIG and IrMn.
- [20] R. F. L. Evans, W. J. Fan, P. Chureemart, T. A. Ostler, M. O. A. Ellis, and R. W. Chantrell, *J. Phys.: Condens. Matter* **26**, 103202 (2014)
- [21] J. Nogues and I. K. Schuller, *J. Magn. Magn. Mater.* **192**,

- 203(1999)
- [22] M. D. Stiles and R. D. McMichael, *Phys. Rev. B* **59**, 3722(1999)
- [23] H. Chen, Q. Niu, and A. H. MacDonald, *Phys. Rev. Lett.* **112**, 017205(2014)
- [24] S. Meyer, R. Schlitz, S. Geprägs, M. Opel, H. Huebl, R. Gross, and S. T. B. Goennenwein, *Appl. Phys. Lett.* **106**, 132402 (2015)
- [25] S. R. Marmion, M. Ali, M. McLaren, D. A. Williams, and B. J. Hickey, *Phys. Rev. B* **89**, 220404(2014)
- [26] X. Zhou, L. Ma, Z. Shi, G. Y. Guo, J. Hu, R. Q. Wu, and S. M. Zhou, *Appl. Phys. Lett.* **105**, 012408(2014)
- [27] G. Y. Guo, Q. Niu, and N. Nagaosa, *Phys. Rev. B* **89**, 214406(2014)
- [28] S. Shimizu, K. S. Takahashi, T. Hatano, Masashi Kawasaki, Y. Tokura, and Y. Iwasa, *Phys. Rev. Lett.* **111**, 216803 (2013)
- [29] S. Geprägs, S. Meyer, S. Altmannshofer, M. Opel, F. Wilhelm, A. Rogalev, R. Gross, and S. T. B. Goennenwein, *Appl. Phys. Lett.* **101**, 262407(2012)
- [30] Y. T. Chen, S. Takahashi, H. Nakayama, M. Althammer, S. T. B. Goennenwein, E. Saitoh, and G. E. W. Bauer, *Phys. Rev. B* **87**, 144411(2013)
- [31] P. Merodio, A. Ghosh, C. Lemonias, E. Gautier, U. Ebels, M. Chshiev, H. Béa, V. Baltz, and W. E. Bailey, *Appl. Phys. Lett.* **104**, 032406 (2014)
- [32] J. C. Rojas-Sánchez, N. Reyren, P. Laczkowski, W. Savero, J.-P. Attané, C. Deranlot, M. Jamet, J.-M. George, L. Vila, and H. Jaffrès, *Phys. Rev. Lett.* **112**, 106602(2014)
- [33] R. Acharyya, H. Y. T. Nguyen, W. P. Pratt, and J. Bass, *J. Appl. Phys.* **109**, 07C503 (2011)
- [34] J. B. S. Mendes, R. O. Cunha, O. Alves Santos, P. R. T. Ribeiro, F. L. A. Machado, R. L. Rodríguez-Suárez, A. Azevedo, and S. M. Rezende, *Phys. Rev. B* **89**, 140406(2014)
- [35] A. Sakuma, K. Fukamichi, K. Sasao, and R. Y. Umetsu, *Phys. Rev. B* **67**, 024420(2003)
- [36] K. Xia, P. J. Kelly, G. E. W. Bauer, A. Brataas, and I. Turek, *Phys. Rev. B* **65**, 220401(2002)